Genomics Proteomics Bioinformatics 20 (2022) 101–109

Genomics Proteomics Bioinformatics

www.elsevier.com/locate/gpb
www.sciencedirect.com

ORIGINAL RESEARCH

Epithelial Cells in 2D and 3D Cultures Exhibit Large Differences in Higher-order Genomic Interactions

Xin Liu [1,#], Qiu Sun [2,#], Qi Wang [3,#], Chuansheng Hu [1], Xuecheng Chen [2], Hua Li [1], Daniel M. Czajkowsky [1,*], Zhifeng Shao [1,*]

[1] *State Key Laboratory for Oncogenes and Bio-ID Center, School of Biomedical Engineering, Shanghai Jiao Tong University, Shanghai 200240, China*
[2] *Shanghai Center for Systems Biomedicine, Shanghai Jiao Tong University, Shanghai 200240, China*
[3] *Translational Medical Center for Stem Cell Therapy & Institute for Regenerative Medicine, Shanghai East Hospital, School of Life Science and Technology, Shanghai Key Laboratory of Signaling and Disease Research, Tongji University, Shanghai 200092, China*

Received 22 August 2019; revised 9 March 2020; accepted 9 August 2020
Available online 23 February 2021

Handled by Giacomo Cavalli

KEYWORDS

3D culture;
In situ Hi-C;
Chromosome conformation;
Compartment;
TAD

Abstract Recent studies have characterized the genomic structures of many eukaryotic cells, often focusing on their relation to gene expression. However, these studies have largely investigated cells grown in 2D cultures, although the transcriptomes of 3D-cultured cells are generally closer to their *in vivo* phenotypes. To examine the effects of spatial constraints on **chromosome conformation**, we investigated the genomic architecture of mouse hepatocytes grown in 2D and **3D cultures** using ***in situ* Hi-C**. Our results reveal significant differences in higher-order genomic interactions, notably in **compartment** identity and strength as well as in topologically associating domain (**TAD**)–TAD interactions, but only minor differences are found at the TAD level. Our RNA-seq analysis reveals up-regulated expression of genes involved in physiological hepatocyte functions in the 3D-cultured cells. These genes are associated with a subset of structural changes, suggesting that differences in genomic structure are critically important for transcriptional regulation. However, there are also many structural differences that are not directly associated with changes in gene expression, whose cause remains to be determined. Overall, our results indicate that growth in 3D significantly alters higher-order genomic interactions, which may be consequential for a subset of genes that are important for the physiological functioning of the cell.

* Corresponding authors.
E-mail: dczaj@sjtu.edu.cn (Czajkowsky DM), zfshao@sjtu.edu.cn (Shao Z).
# Equal contribution.

Peer review under responsibility of Beijing Institute of Genomics, Chinese Academy of Sciences / China National Center for Bioinformation and Genetics Society of China.

https://doi.org/10.1016/j.gpb.2020.06.017

Introduction

The importance of genome structure on the functioning of the genome has now been well established [1–5]. In recent years, perhaps foremost among the methods used to this end are those based on the chromosome conformation capture techniques, most notably *in situ* Hi-C [6]. Such work has revealed a hierarchy of structural features, from locally compact, so-called topologically associating domains (TADs) to more distant TAD–TAD interactions, including broad multi-megabase regions called compartments that are designated as A or B, associated with transcriptionally active or inactive chromatin [7,8]. Although the underlying mechanisms driving the formation of both TADs and compartments are still incompletely understood, their conservation among different cell types and across species suggests that they constitute fundamental components of the eukaryotic genome architecture [4,9,10].

One of the major focuses of previous work has been the determination of the relationship between the genome structure and gene expression [11–14]. Indeed, there have been well-described changes at both the TAD and compartment levels that are significantly related to the transcriptional statuses of genes contained therein [15–17]. Still, there are recent examples of clear differences in gene expression with no detectable changes in the corresponding Hi-C data [18,19], indicating that there can be more complex determinants of the genome structure than just the transcriptional status.

However, to date, almost all of these studies have focused on the genome structures of cultured cells, either immunological cells grown in suspension or, more commonly, adherent cells grown in two-dimensional (2D) cultures [6,20–22]. Such systems are unquestionably powerful to identify biologically important proteins as well as the functions of these proteins in regulating chromosome structure. However, there is still the question of whether or not the overall structures of the genomes in the adherent cells as determined by 2D cultures are applicable to their *in vivo* counterparts. Cells within tissues contact other cells and extracellular matrix components in three dimensions (3D), which can affect gene expression and chromatin conformation [23].

In this regard, there are now well-established methods for culturing cells in 3D [24–26], and indeed the 3D-cultured cells exhibit transcriptomes and cellular behaviors that are more typical of cells within their physiological environment [27–29]. The overall cell shape and the nuclear shape of cells grown in 3D are also often significantly different from the same type of cells grown in 2D [30,31]. Such differences in nuclear shape, in particular, suggest that there are likewise differences in the interactions between whole chromosomes, if not also in the structural details at the sub-chromosomal level. However, the nature of these differences and their relation to differences in transcription have not been well examined. In fact, to our knowledge, the only published Hi-C study which focused on characterizing the differences in genome structure between cells grown in 2D and 3D examined fibroblast cells [30], whose nuclear shape only differs marginally when grown in 2D or 3D (15% change in volume; see Figure S2 in [30]). This work indeed identified differences in genome structure, although at a relatively low resolution of 1 Mb, which is too low to resolve the majority of TADs (median length 185 kb [6]). However, the generality of these results, especially to cells of an epithelial origin, and details of the changes in genomic structure more locally have not yet been elucidated. Moreover, how these changes in genome structure between cells cultured in 2D and 3D relate to the changes in gene expression is also poorly documented.

Here, we examined the genome structures of mouse hepatocytes cultured under 2D and 3D conditions and their relation to gene expression using RNA sequencing (RNA-seq) and *in situ* Hi-C (at a resolution of 40 kb). Overall, we find that the 3D conformation of the genome is clearly different from the 2D conformation but, unexpectedly, only in terms of higher-order interactions, not at the local TAD-level. Nonetheless, a subset of the structural changes in the 3D-cultured cells is associated with the up-regulation of genes that are involved in typical functions of hepatocytes. Thus, growth dimension indeed influences not only cell behavior and transcriptome but also the genome structure, which appears to play a role in effectuating the physiological phenotype of the cell.

Results

In situ Hi-C of hepatocytes cultured under 2D and 3D conditions

To investigate the effects of growth dimension on cell growth, we performed *in situ* Hi-C on alpha mouse liver 12 (AML12) cells, a mouse hepatocyte cell line, grown in either 2D or 3D conditions (**Figure 1**A). For the latter, cells were grown in Matrigel-embedded 3D cultures, which contain extracellular matrix components that are important regulators of normal homeostasis and tissue phenotype [32,33]. Since chromatin structures are known to change significantly during the cell cycle [34], we arrested the cells grown under both conditions at the G1/S boundary using hydroxyurea, an inhibitor of DNA replication [35]. The G1/S state of these cells was confirmed using flow cytometry (Figure S1A).

Consistent with previous reports, we found that the morphological features of the cells were significantly different when grown in 2D or 3D [36]. In particular, while the 2D-cultured cells grew as a single layer, the 3D-cultured cells grew as many individual 3D spheroids with extensive and multiple contacts between the cells (Figure S1B and C). Moreover, the overall cell shape and the nuclear shape of the 2D-cultured cells were significantly different from those of the 3D-cultured cells (Figure 1B and C, Figure S1D and E). Quantitatively, we found that the mean volume of the nuclei of the 2D-cultured cells was nearly twice that of the 3D-cultured cells ($875 \pm 71\ \mu m^3$ and $362 \pm 35\ \mu m^3$, respectively). Such a difference was much more significant than that previously observed in fibroblast cells [30]. Owing to the influence of volume on the T4 DNA ligase efficiency, we adjusted the experimental conditions to optimize the ligation efficiency for Hi-C under our conditions (Figure S1F; see Materials and methods for details).

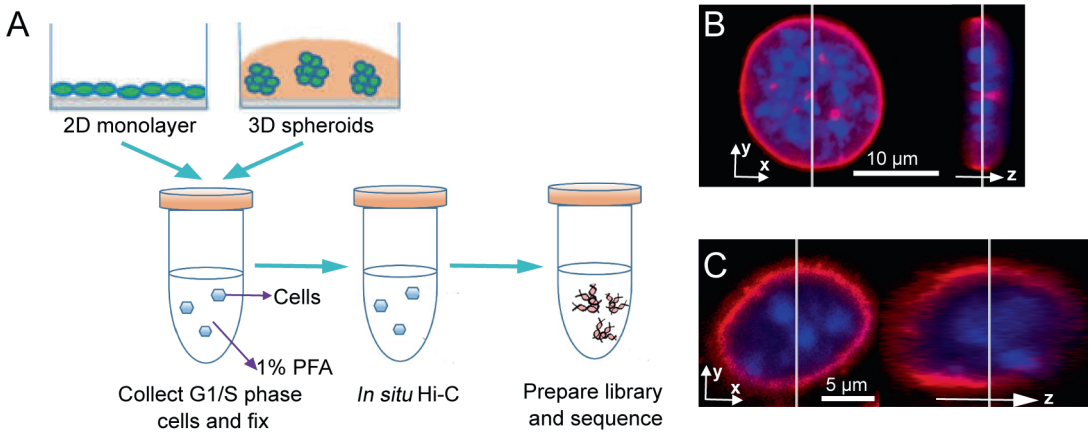

Figure 1 Overview of the experiment

A. Workflow of the experiment. **B.** and **C.** Confocal microscopy images of the 2D-cultured (B) and 3D-cultured (C) mouse AML12 hepatocytes stained with DAPI (blue) and fluorescent antibodies for lamina B (red). PFA, paraformaldehyde.

Overview of the chromatin organization of hepatocytes cultured in 2D and 3D

After sequencing the Hi-C libraries, we generated 214 million and 156 million raw reads, yielding 71 million and 68 million valid paired-end reads after all filtration steps, of the 2D- and 3D-cultured cells, respectively, following a previously described protocol [37]. To evaluate the reliability of our data, we examined a biological replicate for each culture condition, and generated 195 million and 143 million raw reads which finally yielded 80 million and 61 million valid paired-end reads of the 2D- and 3D-cultured cells, respectively (Table S1). Both cultured cells were highly correlated with their corresponding biological replicate with the stratum-adjusted correlation coefficient (SCC) of 0.98 for 2D and 0.97 for 3D, determined using HiCRep [38] (Figure S2A–C; Table S1). Furthermore, a principal component analysis (PCA) of the individual biological replicates also confirmed their high degree of similarity (Figure S2D). Consequently, we combined both of these datasets for our subsequent analyses, obtaining 151 million and 129 million paired-end reads for the 2D- and 3D-cultured cells, respectively, with an estimated highest map resolution of 40 kb for both [6].

Inspection of the Hi-C heatmaps of these cells revealed clear differences in genomic structure at a longer-length scale (**Figure 2**A, Figure S2E and F). However, at the highest resolution of 40 kb, the heatmaps in close proximity to the diagonal (reflecting local interactions such as TADs), were virtually indistinguishable (Figure 2A). Consistent with this observation, the Hi-C datasets at this resolution were highly correlated (Figure 2B; SCC = 0.92).

Comparative examination of the genome structures at the TAD level

We annotated both datasets using the Armatus software [39], and identified a similar number of TADs in both cases (4467 and 4355 TADs in the 2D- and 3D-cultured cells, respectively). The size range and the median size of the identified TADs were also highly consistent under both conditions (median length: 240 kb for the 2D-cultured cells and 280 kb for the

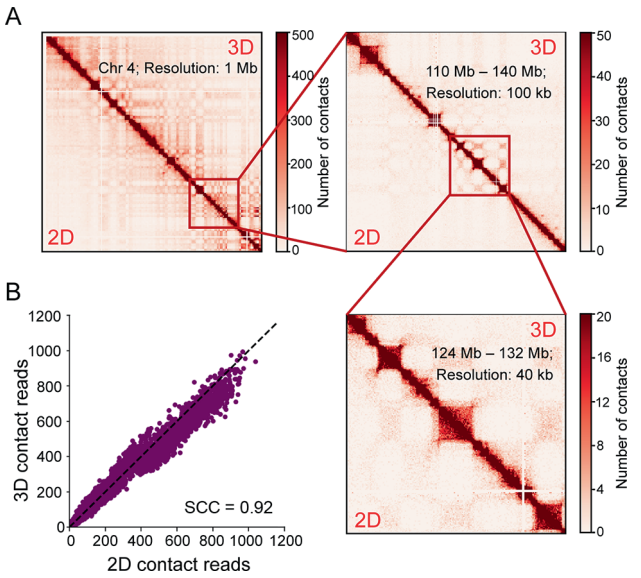

Figure 2 Hi-C measurements of the 2D- and 3D-cultured AML12 cells

A. Heatmaps with increasing resolution as indicated. **B.** Comparison of the contact reads per 40 kb bin. SCC, stratum-adjusted correlation coefficient.

3D-cultured cells; **Figure 3**A; Table S2). These values are also roughly similar to those of earlier studies of other 2D-cultured cells [6,8,40]. Strikingly, the vast majority (>90%) of the TAD borders of these cells overlapped within the limits of our resolution (Figure 3B). Thus, at the TAD level, the genome structures of these hepatocytes are not significantly influenced by the cell culture growth dimension.

Characterization of the genome structures at the compartment level

Since higher-order interactions are also an important aspect of chromosome conformation with functional consequences [41,42], we further characterized the composition of the A/B compartments of the genomes under 2D and 3D conditions

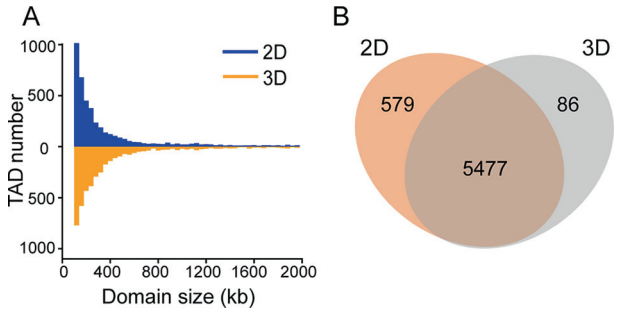

Figure 3 Characterization of the TAD-level features of the 2D- and 3D-cultured cells

A. Size distribution of the TADs annotated from the 40 kb resolution maps. **B.** Venn diagram of the TAD borders of the 2D- and 3D-cultured cells. TAD, topologically associating domain.

(**Figure 4**A; Table S3). As shown in Figure 4B, significant differences are apparent at this level, most notably in the compartment type and the magnitude of intra-compartment contact frequency.

In particular, we found that 1490 compartments (~ 6% of all compartments; determined at a 100 kb resolution) are of a different type between the 2D- and 3D-cultured cells (Figure 4C). Since this difference is markedly higher than those between biological replicates ($P = 1.25 \times 10^{-198}$, Chi-squared test) (Figure S3A and B), the different organization between two conditions is not only significant but also likely consequential. Interestingly, most of these differences (~ 72%) reflect regions that are A compartments in the 2D-cultured cells but are B compartments in the 3D-cultured cells.

As for the differences in the magnitude of intra-compartment contact frequency, we found a difference between the A and B compartments. Of all the possible combinations (A-A, A-B/B-A, and B-B) in the 2D/3D-cultured cells, only the B compartments that are in common between 2D- and 3D-cultured cells (B-B) differed in interaction strength, with those of the 3D-cultured cells exhibiting a greater level of intra-compartment contacts than those of the 2D-cultured cells (Figure 4D; Figure S3C). Consistent with this result, there was also a significantly enriched level of inter-TAD contacts, specifically within the B compartments (Figure S4A and B). These results were also observed when we first normalized the 2D and 3D data jointly (Figure S5), indicating that these results were not caused by technical, condition-specific biases in these samples [43]. Thus, while these genomes were essentially identical at a local TAD level, there were considerable

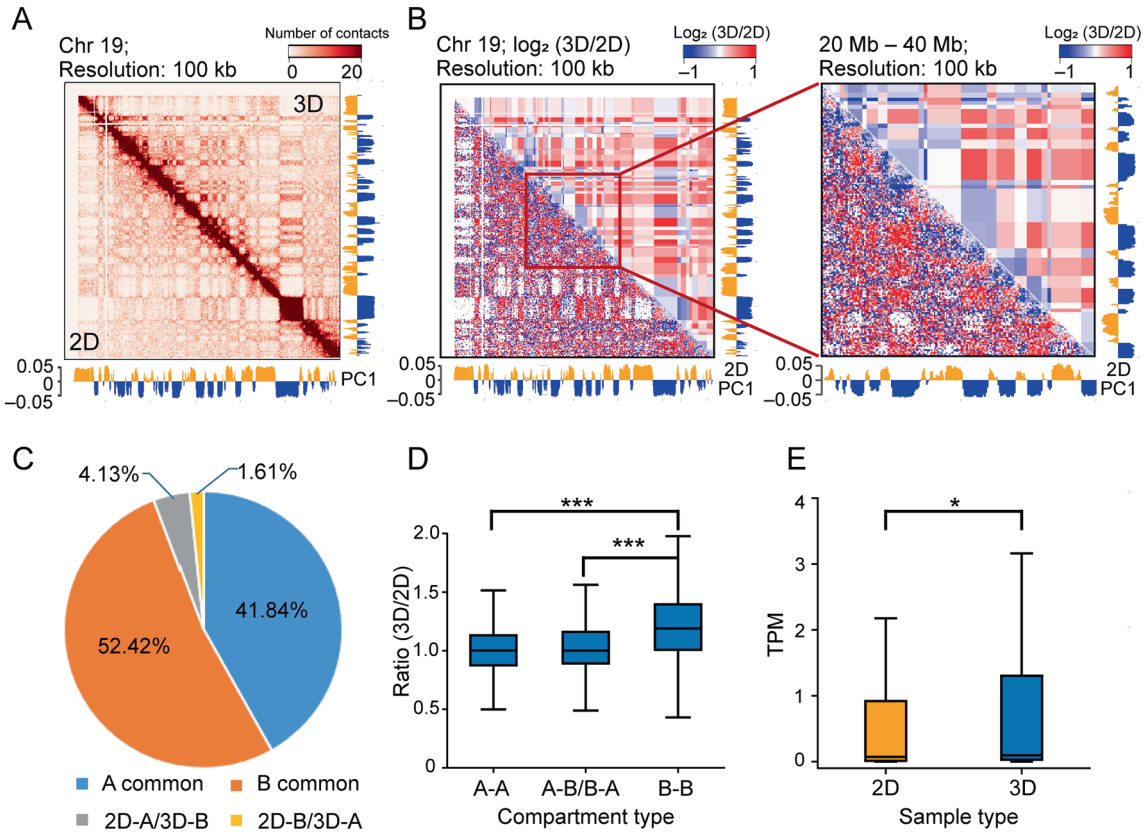

Figure 4 Comparison of the compartment differences between the 2D- and 3D-cultured cells

A. A typical example of a heatmap at the 100 kb resolution, together with the calculated PC1 values used to identify compartments. **B.** Example of the differences in contacts within the compartments. Red and blue represent higher and lower contact frequencies in the 3D-cultured cells, respectively, compared to the 2D-cultured cells. **C.** Pie chart showing the percentages of compartments of a different type between 2D- and 3D-cultured cells. The compartments that have changed types are described according to their designation in the 2D-cultured cells (A or B) changing to that in the 3D-cultured cells (B or A). **D.** Box plot showing the changes in intra-compartment contacts between 2D- and 3D-cultured cells. **E.** Box plot showing the expression changes for genes that are in a B compartment in the 2D-cultured cells but in an A compartment in the 3D-cultured cells. *, $P < 0.05$; ***, $P < 0.001$ (Wilcoxon rank sum test). PC1, first principal component; TPM, transcripts per million.

differences at the higher-order scale, especially within the B compartments that were in common between 2D- and 3D-cultured cells.

Comparison between transcriptional and genomic structural changes

Based on the commonly observed relationship between transcription levels and genomic structures, particularly at the TAD level, and the high similarity of genomic structures at the TAD level described above, we expected that there might be only a few expression differences between the 2D- and 3D-cultured cells. To verify this hypothesis, we performed an RNA-seq analysis of the cells grown in 2D and 3D in parallel. Contrary to our expectation, more than a thousand genes exhibited significantly different expression in the 3D-cultured cells, including 674 up-regulated genes and 592 down-regulated genes, when compared to the 2D-cultured cells ($P < 0.05$, $|\log_2 \text{fold change}| > 2$). Interestingly, Gene Ontology (GO) analysis showed that the genes that were up-regulated in the 3D-cultured cells were enriched in the terms related to the physiological functions of the hepatocytes (particularly metabolic functions) (Figure S6A; Table S4), in agreement with common expectations [44–46]. Notably, these genes were not preferentially up-regulated in the 3D-cultured fibroblast cells compared with those cultured in 2D [30].

To examine the possible relationship between gene expression levels and genomic structures at the TAD level, we investigated the expression differences of the genes in the TADs which were shared by the 2D- and 3D-cultured cells but had different contact frequencies. However, we found no significant difference in the expression of the genes in these TADs in the 2D- and 3D-cultured cells (Figure S7A and B).

A similar analysis at the compartment level, however, showed significant differential gene expression within the compartments which were B-type in the 2D-cultured cells but A-type in the 3D-cultured cells (2D-B/3D-A; $P < 0.05$, Wilcoxon rank sum test; Figure 4E). Notably, there was an enrichment of genes that were up-regulated in the 2D-B/3D-A compartments of the 3D-cultured cells, and these genes were associated with the physiological functions of hepatocytes (Figure S6B and C; Table S5). However, examination for the correlation between transcriptional changes and other compartment-level features (*i.e.*, A common, B common, and 2D-A/3D-B) did not identify any enrichment of genes with differential expression (Figure S8A–C). Nonetheless, the up-regulation of the genes associated with the physiological functions of hepatocytes in the 3D-cultured cells appeared to be related to the changes in the compartment-level genomic structures of these cells (Figure S9).

Discussion

In this study, we investigated the genomic structure and the transcriptome of hepatocytes cultured under 2D and 3D conditions, and examined whether these structural differences correlate with changes in gene expression. This first comparison of the genomic structures of cells grown under these different conditions at the sub-TAD resolution reveals several features of chromosome architecture, particularly with regard to its relationship with gene expression.

First, we find that, at the local TAD level, the architecture of the genomes of the 2D- and 3D-cultured cells is highly similar despite the differences in their transcriptomes. Although the underlying mechanisms driving the formation of TADs are still being uncovered, our observations clearly indicate that they are not exquisitely sensitive to the growth dimension of the cells or to the profound differences in nuclear shape or volume we observed. Furthermore, the absence of any significant correlation between TAD-level structures and the differences in gene expression between 2D- and 3D-cultured cells also indicates that these mechanisms are not highly dependent on, or related to, the transcriptional statuses of genes contained therein. Recent studies have also described a lack of close correlation between changed transcriptomes and differences in Hi-C data at the TAD level [19,47,48]. Whether this reflects a change in histone modifications within an essentially similar genomic structure [20,49–51] or other mechanisms requires further investigation.

Second, we observe significant differences between 2D- and 3D-cultured cells in higher-order interactions, from TAD–TAD interactions to entire compartments. Some of these differences are associated with differential gene expression between two culture conditions. Furthermore, the correlation between the up-regulation of genes involved in physiological hepatocyte functions in the 3D-cultured cells and the change of genome structure from a B (inactive) compartment in the 2D-cultured cells to an A (active) compartment in the 3D-cultured cells, strongly suggests that some of these structural changes are required to effectuate the more physiological phenotype of the 3D-cultured cells. However, the identification of many structural changes that are not correlated with the changed gene expression suggests that these structural changes could play roles other than gene regulation, an observation that is becoming better appreciated [18,19,52].

In conclusion, our work demonstrates the importance of characterizing the genome structure of cells grown under conditions that yield a more physiological phenotype. The genome structure is fundamentally different in cells grown under 2D and 3D conditions, and this difference appears to be consequential to the physiological functioning of the cells. While the ideal sample to investigate are cells within their native tissue, our work shows that culturing cells in 3D provides a readily attainable and highly effective system for this purpose.

Materials and methods

Cell culture, synchronization, and crosslinking

AML12 cells (Stem Cell Bank, Chinese Academy of Sciences, Shanghai, China) were cultured in a mix of Dulbecco's modified Eagle's medium and Ham's F12 medium (1:1) containing 10% fetal calf serum and supplied with 1× ITS liquid media supplement [10 μg/ml recombinant human insulin, 5.5 μg/ml human transferrin (substantially iron-free), 5 ng/ml sodium selenite (Catalog No. I3146, Sigma-Aldrich, St. Louis, MO), 40 ng/ml dexamethasone (Catalog No. D4902, Sigma-Aldrich), 100 U/ml penicillin–streptomycin (Catalog No. 11548876, Gibco, Carlsbad, CA)] at 37 °C for 48 h. Then, the cells were dissociated with 0.25% trypsin to suspend them for re-plating. For the 2D cultures, cells were re-plated in 10-cm dishes. For the 3D cultures, cells were grown in

Matrigel-embedded 3D cultures in 10-cm dishes. When the cells in the 2D cultures were 50% confluent and the cells in the 3D cultures had grown for 24 h, 1 mM hydroxyurea was added to the medium for 24-h [53] and 36-h incubations for 2D and 3D conditions, respectively. This difference in incubation time with hydroxyurea was chosen owing to the differences in cell-cycle time under these culture conditions. The 2D-cultured cells were cross-linked directly, and then detached from the Petri dish with 1% paraformaldehyde (PFA) for 4 h at 17 °C while mixing in the Petri dish. The PFA was quenched with glycine at a final concentration of 0.125 M for 15 min at room temperature while mixing. The intact spheroids of the 3D-cultured cells were collected with the Cell Recovery Solution (Catalog No. 354253, Corning, NY), and then fixed following the same procedure used for 2D-cultured cells. The cross-linked cells were pelleted by centrifugation, washed with ice-cold PBS, flash-frozen in liquid nitrogen, and finally stored at −80 °C until the preparation of the *in situ* Hi-C libraries.

Immunofluorescence

For the Lamin B1 staining, the cells were first fixed with 4% PFA at room temperature for 10 min, followed by PFA quenching with glycine at a final concentration of 50 mM. Subsequently, the cells were washed three times with PBS, permeabilized with 0.5% Triton X-100 for 10 min, and then blocked with 5% BSA to reduce non-specific binding. Next, the cells were incubated with the primary antibody, anti-Lamin B1 (1:200; Catalog No. ab16048, Abcam, Cambridge, UK), overnight at 4 °C. The cells were then washed three times with PBS and incubated with the secondary antibody, Donkey anti-Rabbit IgG (H + L) Highly Cross-Adsorbed Secondary Antibody, Alexa Fluor 568 (1:200; Catalog No. A10042, ThermoFisher Scientific, Waltham, MA) for 1 h at room temperature. Finally, the nuclei were stained with DAPI (1 μg/ml). For staining of the plasma membrane, the sample was fixed, permeabilized, and blocked as previously described, and then incubated with Wheat Germ Agglutinin, Alexa Fluor 555 conjugate (1:200; Catalog No. W32464, ThermoFisher Scientific) for 30 min at room temperature. All imaging was performed with confocal fluorescence microscopy (A1Si, Nikon, Japan) at a scan speed of 1/4 frames/s.

Hi-C library preparation

The cells were thawed on ice and re-suspended into ice-cold lysis buffer [10 mM Tris-HCl pH 8.0, 10 mM NaCl, 0.2% Triton X-100, 1/100 volume of the proteinase inhibitor cocktail (Catalog No. P8340, Sigma-Aldrich)]. Following incubation on ice for 30 min, the nuclei were pelleted and washed with ice-cold lysis buffer. After washing with 1.2× cutsmart buffer (Catalog No. B7204, NEB, Ipswich, MA), the nuclei were re-suspended with 1.2× cutsmart buffer supplemented with 0.1% SDS and incubated for 1 h at 65 °C. After, the nuclei were incubated with 1% Triton X-100 for 15 min at 37 °C, and then digested overnight at 37 °C with 100 U of restriction endonuclease *Mbo*I (5 U/μl; Catalog No. R0147, NEB) with slow rotation.

The nuclei were pelleted and washed twice with 1× NEBuffer 2 (Catalog No. B7002, NEB). The nuclei were then re-suspended with 1× NEBuffer 2 containing 0.015 mM dCTP, 0.015 mM dGTP, 0.015 mM dTTP, 0.015 mM biotin-14-dATP, and 5 U of Klenow enzyme (Catalog No. M0210, NEB). The mixture was incubated at 37 °C for 2 h with slow rotation. Next, the nuclei were harvested and re-suspended in the ligation master mix [1× T4 ligase buffer (NEB), 0.1 mg/ml BSA, 40 U/μl of T4 ligase (Catalog No. B0202, NEB) in ddH_2O], followed by incubation at 25 °C for 4 h and 16 °C for 8 h. The crosslinking was then reversed by incubating overnight at 65 °C with proteinase K (1 μg/μl). The DNA was extracted with phenol–chloroform and purified with ethanol precipitation. Then, the RNA was removed by RNase A (1 μg/μl), and the DNA was sheared with Covaris M220. The DNA fraction in the size range of 300–500 bp was collected with Agencourt AMPure XP beads (Catalog No. A63881, Beckman Coulter, Brea, CA).

The DNA was end-repaired and 'A' tailed with the "NEBNext End Pre" module, and adapters were ligated with the "Adaptor ligation" module in the NEBNext Ultra DNA Library Prep Kit for Illumina (Catalog No. E7370, NEB) according to the manufacturer's instructions. Subsequently, biotin-mediated pull-down of the ligation products was performed as previously described [6] with minor modification. Then, the DNA suspension was transferred into a PCR tube and PCR amplified with index primers, universal PCR primers, and the NEBNext High Fidelity 2× PCR Master Mix. The PCR reactions were performed following the manufacturer's instructions of the NEBNext Ultra DNA Library Prep Kit for Illumina (Catalog No. E7370, NEB). The concentrations of the Hi-C libraries were determined using the Qubit dsDNA HS Assay, and the quality was measured by Agilent 2100 DNA 1000 HS Kit. Lastly, the high-quality libraries were sequenced using an Illumina X-ten platform with 150 bp paired-end reads.

Hi-C data processing

We mapped all Hi-C reads to the mm10 mouse reference genome using Bowtie 2 (v2.2.9) iteratively as described [37]. For each end of the Hi-C reads, we first mapped an outermost length of 30 bp, and if this length of region failed to map uniquely, we included an additional 20 bp in the next round of mapping. This procedure continued until the mapping length reached the full read length of 150 bp. Read pairs with mapping quality (MAPQ) larger than 30 for each end were kept. Then, the reads mapped to the same restriction fragment and the dangling reads having a separating genomic distance shorter than 500 bp were removed. We generated Hi-C contact matrices at 1 Mb, 100 kb, or 40 kb resolutions for each chromosome and normalized using ICE [54]. To test the validity of our data, we calculated the SCC [38] between the biological replicates of the 2D- and 3D-cultured cells, respectively. For comparison, we selected the same number (35 M) of intra-chromosomal reads for each replicate of the 2D- and 3D-cultured cells. The fractions of *trans*-interactions among the valid reads for the 2D and 3D datasets were ~ 32% and ~ 43%, respectively, within the range (27%–57%) of several recently published Hi-C datasets [20,55–59]. Furthermore, these percentages were highly consistent between individual biological replicates (31%/32% for 2D and 42%/43% for 3D).

Annotation of the compartments and TADs

We annotated the compartments at a 100 kb resolution as previously described [7]. Specifically, we performed a PCA of the normalized contact matrix for each chromosome, and assigned the signs of the first principal component (PC1) to different types of compartments. To determine the signs of the PC1, we calculated the Pearson correlation coefficient (PCC) between the eigenvectors and the read densities of RNA-seq of the corresponding regions. If the PCC was negative, the eigenvector was multiplied by −1. Positive values of the PC1 defined A-type compartments and negative ones defined B-type.

To reduce the bias introduced by the differences in sequencing depth, we normalized the total contact numbers of each chromosome in the 2D and 3D datasets to the same depth before annotating the domains. After the depth normalization, we annotated the domains using the software Armatus v1.0 [39,60] with the gamma parameter set to 0.8.

Calculation of the compartment–compartment and TAD–TAD contact enrichment

For each pair of compartments and TADs, we calculated the average contact frequencies of all pairs of bins with gap bins excluded. We removed the compartment and TAD pairs if the number of gap bin pairs took more than 50% of the total bin pairs within the corresponding compartments or TADs. The average contact frequencies of TAD–TAD or compartment–compartment pairs between 2D- and 3D-cultured cells were then calculated.

RNA-seq library construction

Total RNA was extracted from 3 million cells using Trizol Reagent, and the quality was assessed using Agilent Bioanalyzer 2100. The RNA-seq libraries were prepared using the KAPA Stranded mRNA-seq Kit (Catalog No. 07962193001, Roche, Basel, Switzerland) following the manufacturer's instructions. The quality of the libraries was measured by the Qubit fluorometer and Agilent Bioanalyzer 2100. The libraries were then sequenced with the Illumina X-ten platform (2 × 150).

RNA-seq data analysis and functional annotation

We removed adapters and low-quality reads using cutadapt (v1.8.3) [61] and Trimmomatic (v0.36) [62] with default parameters. The remaining valid paired reads were mapped to the GRCm38 mouse reference genome by HISAT2 (v2.0.5) [63] with options "--rna-strandness RF --no-softclip". We next assembled and quantified the transcripts using Stringtie (v1.3.4) [64] with the Mus_musculus.GRCm38.93.chr GTF file downloaded from the Ensembl database. The read counts of the detected genes were extracted from the output files of Stringtie through the Python script "prepDE.py" provided online (https://ccb.jhu.edu/software/stringtie/dl/prepDE.py). To evaluate the difference in gene expression between 2D- and 3D-cultured cells, we used the R package "DESeq2" [65] to calculate the fold change of the transcription levels and assigned a statistical significance to each pair of genes. Genes with $|\log_2$ fold change$| > 2$ and $P < 0.05$ were identified as differentially expressed genes. The GO terms for the gene functional classification were determined using DAVID (v6.8) (https://david.ncifcrf.gov/gene2gene.jsp).

Data availability

The Hi-C and RNA-seq datasets in this study have been deposited at the Gene Expression Omnibus (GEO: GSE136307) that are publicly accessible at https://www.ncbi.nlm.nih.gov/geo, and in the Genome Sequence Archive [66] at the National Genomics Data Center, Beijing Institute of Genomics, Chinese Academy of Sciences / China National Center for Bioinformation (GSA: CRA002599) that are publicly accessible at https://ngdc.cncb.ac.cn/gsa.

CRediT author statement

Xin Liu: Investigation, Methodology, Writing - original draft. **Qiu Sun:** Software, Formal analysis, Data curation, Writing - review & editing. **Qi Wang:** Investigation, Methodology, Writing - review & editing. **Chuansheng Hu:** Formal analysis. **Xuecheng Chen:** Investigation. **Hua Li:** Formal analysis. **Daniel M. Czajkowsky:** Conceptualization, Formal analysis, Writing - original draft. **Zhifeng Shao:** Conceptualization, Methodology, Writing - original draft. All authors have read and approved the final manuscript.

Competing interests

The authors have declared no competing interests.

Acknowledgments

This work was supported by the grants from the National Key R&D Program of China (Grant No. 2018YFC1003500), the National Natural Science Foundation of China (Grant Nos. 11374207, 31501054, 31670722, 31971151, 81627801, and 31900430), and the China Postdoctoral Science Foundation (Grant No. 2018M640419). We are also grateful for the generous support from Nikon Instruments (Shanghai) Co., Ltd.

Supplementary material

Supplementary material to this article can be found online at https://doi.org/10.1016/j.gpb.2020.06.017.

ORCID

ORCID 0000-0002-0246-0313 (Xin Liu)
ORCID 0000-0003-1379-6637 (Qiu Sun)
ORCID 0000-0001-8468-5649 (Qi Wang)
ORCID 0000-0001-9685-9220 (Chuansheng Hu)
ORCID 0000-0001-6796-9455 (Xuecheng Chen)
ORCID 0000-0003-2153-2500 (Hua Li)
ORCID 0000-0002-2745-9546 (Daniel M. Czajkowsky)
ORCID 0000-0002-2147-6652 (Zhifeng Shao)

References

[1] Reddy KL, Zullo JM, Bertolino E, Singh H. Transcriptional repression mediated by repositioning of genes to the nuclear lamina. Nature 2008;452:243.

[2] Ried T, Rajapakse I. The 4D Nucleome. Methods 2017;123:1.

[3] Seaman L, Chen H, Brown M, Wangsa D, Patterson G, Camps J, et al. Nucleome analysis reveals structure–function relationships for colon cancer. Mol Cancer Res 2017;15:821–30.

[4] Dixon JR, Jung I, Selvaraj S, Shen Y, Antosiewiczbourget JE, Lee AY, et al. Chromatin architecture reorganization during stem cell differentiation. Nature 2015;518:331–6.

[5] Bunting KL, Soong TD, Singh R, Jiang Y, Béguelin W, Poloway DW, et al. Multi-tiered reorganization of the genome during B cell affinity maturation anchored by a germinal center-specific locus control region. Immunity 2016;45:497–512.

[6] Rao SS, Huntley MH, Durand NC, Stamenova EK, Bochkov ID, Robinson JT, et al. A 3D map of the human genome at kilobase resolution reveals principles of chromatin looping. Cell 2014;159:1665–80.

[7] Lieberman-Aiden E, Van Berkum NL, Williams L, Imakaev M, Ragoczy T, Telling A, et al. Comprehensive mapping of long-range interactions reveals folding principles of the human genome. Science 2009;326:289–93.

[8] Dixon JR, Selvaraj S, Yue F, Kim A, Li Y, Shen Y, et al. Topological domains in mammalian genomes identified by analysis of chromatin interactions. Nature 2012;485:376.

[9] Stevens TJ, Lando D, Basu S, Atkinson LP, Cao Y, Lee SF, et al. 3D structures of individual mammalian genomes studied by single-cell Hi-C. Nature 2017;544:59.

[10] Schmitt AD, Hu M, Jung I, Xu Z, Qiu Y, Tan CL, et al. A compendium of chromatin contact maps reveals spatially active regions in the human genome. Cell Rep 2016;17:2042–59.

[11] Whalen S, Truty RM, Pollard KS. Enhancer–promoter interactions are encoded by complex genomic signatures on looping chromatin. Nat Genet 2016;48:488.

[12] Pope BD, Ryba T, Dileep V, Yue F, Wu W, Denas O, et al. Topologically associating domains are stable units of replication-timing regulation. Nature 2014;515:402.

[13] Dekker J, Mirny L. The 3D genome as moderator of chromosomal communication. Cell 2016;164:1110–21.

[14] Lucas JS, Zhang Y, Dudko OK, Murre C. 3D trajectories adopted by coding and regulatory DNA elements: first-passage times for genomic interactions. Cell 2014;158:339–52.

[15] Andrey G, Montavon T, Mascrez B, Gonzalez F, Noordermeer D, Leleu M, et al. A switch between topological domains underlies HoxD genes collinearity in mouse limbs. Science 2013;340:1234167.

[16] Lupiáñez DG, Kraft K, Heinrich V, Krawitz P, Brancati F, Klopocki E, et al. Disruptions of topological chromatin domains cause pathogenic rewiring of gene-enhancer interactions. Cell 2015;161:1012–25.

[17] Symmons O, Uslu VV, Tsujimura T, Ruf S, Nassari S, Schwarzer W, et al. Functional and topological characteristics of mammalian regulatory domains. Genome Res 2014;24:390–400.

[18] Palstra RJ, Simonis M, Klous P, Brasset E, Eijkelkamp B, De Laat W. Maintenance of long-range DNA interactions after inhibition of ongoing RNA polymerase II transcription. PLoS One 2008;3:e1661.

[19] Jacobson EC, Perry JK, Long DS, Olins AL, Olins DE, Wright BE, et al. Migration through a small pore disrupts inactive chromatin organization in neutrophil-like cells. BMC Biol 2018;16:142.

[20] Phanstiel DH, Van Bortle K, Spacek D, Hess GT, Shamim MS, Machol I, et al. Static and dynamic DNA loops form AP-1-bound activation hubs during macrophage development. Mol Cell 2017;67:1037–48.e6.

[21] Wang S, Su JH, Beliveau BJ, Bintu B, Moffitt JR, Wu CT, et al. Spatial organization of chromatin domains and compartments in single chromosomes. Science 2016;353:598–602.

[22] Liang Z, Li G, Wang Z, Djekidel MN, Li Y, Qian MP, et al. BL-Hi-C is an efficient and sensitive approach for capturing structural and regulatory chromatin interactions. Nat Commun 2017;8:1622.

[23] Storch K, Eke I, Borgmann K, Krause M, Richter C, Becker K, et al. Three-dimensional cell growth confers radioresistance by chromatin density modification. Cancer Res 2010;70:3925–34.

[24] Antoni D, Burckel H, Josset E, Noel G. Three-dimensional cell culture: a breakthrough *in vivo*. Int J Mol Sci 2015;16:5517–27.

[25] Clevers H. Modeling development and disease with organoids. Cell 2016;165:1586–97.

[26] Knight E, Przyborski S. Advances in 3D cell culture technologies enabling tissue-like structures to be created *in vitro*. J Anat 2015;227:746–56.

[27] Choi SH, Kim YH, Hebisch M, Sliwinski C, Lee S, D'Avanzo C, et al. A three-dimensional human neural cell culture model of Alzheimer's disease. Nature 2014;515:274.

[28] Sasai Y. Next-generation regenerative medicine: organogenesis from stem cells in 3D culture. Cell Stem Cell 2013;12:520–30.

[29] Chen H, Seaman L, Liu S, Ried T, Rajapakse I. Chromosome conformation and gene expression patterns differ profoundly in human fibroblasts grown in spheroids *versus* monolayers. Nucleus 2017;8:383–91.

[30] Chen H, Comment N, Chen J, Ronquist S, Hero A, Ried T, et al. Chromosome conformation of human fibroblasts grown in 3-dimensional spheroids. Nucleus 2015;6:55–65.

[31] Lee GY, Kenny PA, Lee EH, Bissell MJ. Three-dimensional culture models of normal and malignant breast epithelial cells. Nat Methods 2007;4:359.

[32] Bissell M, Kenny P, Radisky DC. Microenvironmental regulators of tissue structure and function also regulate tumor induction and progression: the role of extracellular matrix and its degrading enzymes. Cold Spring Harb Symp Quant Biol 2005;70:343–56.

[33] Bissell MJ, Radisky DC, Rizki A, Weaver VM, Petersen OW. The organizing principle: microenvironmental influences in the normal and malignant breast. Differentiation 2002;70:537–46.

[34] Naumova N, Imakaev M, Fudenberg G, Zhan Y, Lajoie BR, Mirny LA, et al. Organization of the mitotic chromosome. Science 2013;342:948–53.

[35] Graham AC, Kiss DL, Andrulis ED. Core exosome-independent roles for Rrp6 in cell cycle progression. Mol Biol Cell 2009;20:2242–53.

[36] Edmondson R, Broglie JJ, Adcock AF, Yang L. Three-dimensional cell culture systems and their applications in drug discovery and cell-based biosensors. Assay Drug Dev Technol 2014;12:207–18.

[37] Wang Q, Sun Q, Czajkowsky DM, Shao Z. Sub-kb Hi-C in *D. melanogaster* reveals conserved characteristics of TADs between insect and mammalian cells. Nat Commun 2018;9:188.

[38] Yang T, Zhang F, Yardımcı GG, Song F, Hardison RC, Noble WS, et al. HiCRep: assessing the reproducibility of Hi-C data using a stratum-adjusted correlation coefficient. Genome Res 2017;27:1939–49.

[39] Filippova D, Patro R, Duggal G, Kingsford C. Identification of alternative topological domains in chromatin. Algorithms Mol Biol 2014;9:14.

[40] Forcato M, Nicoletti C, Pal K, Livi CM, Ferrari F, Bicciato S. Comparison of computational methods for Hi-C data analysis. Nat Methods 2017;14:679.

[41] Miele A, Dekker J. Long-range chromosomal interactions and gene regulation. Mol Biosyst 2008;4:1046–57.

[42] Miele A, Bystricky K, Dekker J. Yeast silent mating type loci form heterochromatic clusters through silencer protein-dependent long-range interactions. PLoS Genet 2009;5:e1000478.

[43] Stansfield JC, Cresswell KG, Vladimirov VI, Dozmorov MG. HiCcompare: an R-package for joint normalization and comparison of HI-C datasets. BMC Bioinformatics 2018;19:279.
[44] Ramaiahgari SC, Den Braver MW, Herpers B, Terpstra V, Commandeur JN, van de Water B, et al. A 3D *in vitro* model of differentiated HepG2 cell spheroids with improved liver-like properties for repeated dose high-throughput toxicity studies. Arch Toxicol 2014;88:1083–95.
[45] Takahashi Y, Hori Y, Yamamoto T, Urashima T, Ohara Y, Tanaka H. 3D spheroid cultures improve the metabolic gene expression profiles of HepaRG cells. Biosci Rep 2015;35:e00208.
[46] Bell CC, Dankers AC, Lauschke VM, Sison-Young R, Jenkins R, Rowe C, et al. Comparison of hepatic 2D sandwich cultures and 3D spheroids for long-term toxicity applications: a multicenter study. Toxicol Sci 2018;162:655–66.
[47] Despang A, Schöpflin R, Franke M, Ali S, Jerkovic I, Paliou C, et al. Functional dissection of TADs reveals non-essential and instructive roles in regulating gene expression. bioRxiv 2019; 566562.
[48] Stadhouders R, Vidal E, Serra F, Di Stefano B, Le Dily F, Quilez J, et al. Transcription factors orchestrate dynamic interplay between genome topology and gene regulation during cell reprogramming. Nat Genet 2018;50:238–49.
[49] Comoglio F, Park HJ, Schoenfelder S, Barozzi I, Bode D, Fraser P, et al. Thrombopoietin signaling to chromatin elicits rapid and pervasive epigenome remodeling within poised chromatin architectures. Genome Res 2018;28:295–309.
[50] Jin F, Li Y, Dixon JR, Selvaraj S, Ye Z, Lee AY, et al. A high-resolution map of the three-dimensional chromatin interactome in human cells. Nature 2013;503:290.
[51] Le Dily F, Baù D, Pohl A, Vicent GP, Serra F, Soronellas D, et al. Distinct structural transitions of chromatin topological domains correlate with coordinated hormone-induced gene regulation. Genes Dev 2014;28:2151–62.
[52] Hug CB, Grimaldi AG, Kruse K, Vaquerizas JM. Chromatin architecture emerges during zygotic genome activation independent of transcription. Cell 2017;169:216–28.e19.
[53] Tian HY, Zhang KH, Gao X, Lei WW, Zhang L, Yu ML, et al. Comparative proteomic analysis of cell cycle-dependent apoptosis induced by transforming growth factor-beta. Biochim Biophys Acta 2009;1794:1387–97.
[54] Imakaev M, Fudenberg G, McCord RP, Naumova N, Goloborodko A, Lajoie BR, et al. Iterative correction of Hi-C data reveals hallmarks of chromosome organization. Nat Methods 2012;9:999.
[55] Hu S, Lv P, Yan Z, Wen B. Disruption of nuclear speckles reduces chromatin interactions in active compartments. Epigenetics Chromatin 2019;12:43.
[56] Du Z, Zheng H, Huang B, Ma R, Wu J, Zhang X, et al. Allelic reprogramming of 3D chromatin architecture during early mammalian development. Nature 2017;547:232.
[57] Ke Y, Xu Y, Chen X, Feng S, Liu Z, Sun Y, et al. 3D chromatin structures of mature gametes and structural reprogramming during mammalian embryogenesis. Cell 2017;170:367–81.e20.
[58] Rudan MV, Barrington C, Henderson S, Ernst C, Odom DT, Tanay A, et al. Comparative Hi-C reveals that CTCF underlies evolution of chromosomal domain architecture. Cell Rep 2015;10:1297–309.
[59] Nagano T, Várnai C, Schoenfelder S, Javierre BM, Wingett SW, Fraser P. Comparison of Hi-C results using in-solution *versus* in-nucleus ligation. Genome Biol 2015;16:175.
[60] Ulianov SV, Khrameeva EE, Gavrilov AA, Flyamer IM, Kos P, Mikhaleva EA, et al. Active chromatin and transcription play a key role in chromosome partitioning into topologically associating domains. Genome Res 2016;26:70–84.
[61] Martin M. Cutadapt removes adapter sequences from high-throughput sequencing reads. EMBnet J 2011;17:10–2.
[62] Bolger AM, Lohse M, Usadel B. Trimmomatic: a flexible trimmer for Illumina sequence data. Bioinformatics 2014;30:2114–20.
[63] Kim D, Langmead B, Salzberg SL. HISAT: a fast spliced aligner with low memory requirements. Nat Methods 2015;12:357.
[64] Pertea M, Pertea GM, Antonescu CM, Chang TC, Mendell JT, Salzberg SL. StringTie enables improved reconstruction of a transcriptome from RNA-seq reads. Nat Biotechnol 2015;33:290.
[65] Love MI, Huber W, Anders S. Moderated estimation of fold change and dispersion for RNA-seq data with DESeq2. Genome Biol 2014;15:550.
[66] Chen T, Chen X, Zhang S, Zhu J, Tang B, Wang A, et al. The Genome Sequence Archive Family: toward explosive data growth and diverse data types. Genomics Proteomics Bioinformatics 2021;19:578–83.